Available online at www.sciencedirect.com
ScienceDirect
Magnetic Resonance Imaging xx (2011) xxx–xxx
MAGNETIC RESONANCE IMAGING

MRI measurements of CO_2 hydrate dissociation rate in a porous medium ☆

Mingjun Yang[a], Yongchen Song[a,*], Yuechao Zhao[a], Yu Liu[a], Lanlan Jiang[a], Qingping Li[b]

[a]Key Laboratory of Ocean Energy Utilization and Energy Conservation of Ministry of Education, Dalian University of Technology, Dalian 116024, China
[b]CNOOC Research Center, Beijing 100027, China

Received 4 March 2011; revised 6 April 2011; accepted 10 April 2011

Abstract

After obtaining experimental data of CO_2 hydrate formation and dissociation in a porous medium using magnetic resonance imaging (MRI), the purpose of this study was to analyze the different dissociation rate of CO_2 hydrate using two heating rates. Images were obtained by using a fast spin-echo sequence, and the field of view was set to 40×40×40 mm. The vessel pressure was monitored during hydrate formation and dissociation, which was used to compare with MRI mean intensity. The result indicated that the MRI could visualize hydrate formation and dissociation, and the MRI mean intensity of water was in good agreement with the vessel pressure changes. The hydrate formation and dissociation rates were also quantified using the MRI mean intensity of water. The experimental results showed that the higher heating rate caused the rapid hydrate dissociation.

Keywords: CO_2 hydrate; Porous medium; MRI; Experiments

1. Introduction

The explosive growth of fossil fuel consumption has caused global problems, including air toxics and greenhouse gases (GHG). CO_2 is the largest contributor in regard of its amount present in the atmosphere contributing to 60% of global warming effects [1]. So sequestration of CO_2 became an important issue, and scientists are exploring the option of sequestering CO_2 in the deep ocean [2]. Since the pressure and temperature conditions in ocean and in marine sediment may well be within the CO_2 hydrate stability zone [3], the CO_2 can be sequestrated in hydrate form, and a number of investigations have been carried out for this topic. Since 1998, Brewer et al. [4–7] had carried out numerous investigations about the behavior of CO_2 and hydrate in seawater and marine sediments. They used a remotely operated vehicle (ROV) to initiate a program of research into gas hydrate formation in the deep sea by controlled release of hydrocarbon gases and liquid CO_2 into natural sea water and marine sediments. Since the ROV can control the depth of release site, they operated a series of in situ experiments in different places. A glass combination pH electrode modified by the manufacturer was deployed at depth to monitor pH [6], and they captured images with a specially modified Sony HDC-750 high-definition television camera which digitizes the picture data and formats it to the SMPTE 292M HDTV interface standard with 2:1 interlace.

Koide et al. [8] analyzed three types of sub-seabed disposal of CO_2, such as shallow, deep and super-deep sub-seabed disposal. They concluded that the shallow sub-seabed disposal of CO_2 in aquifers is technically and economically feasible and safer than inland aquifer disposal. Deep sub-seabed disposal of CO_2 in aquifers under seabed provides the most protective storage for CO_2 thanks to formation of CO_2 hydrate in sub-seabed sediments. Super-deep sub-seabed disposal of CO_2 under light unconsolidated sediments also hardly affects the ecology on the seabed. Aya et al. [9,10], Lee et al. [11], Saji et al. [12] and Yamasaki et al. [13] also carried out several investigations about disposing CO_2 in hydrate form in seawater and marine sediment.

MRI is an effective tool for investigations in physical, chemical, life and clinical sciences as it noninvasively maps

☆ This project is financially supported by the Key Program of the National Natural Science Foundation of China (50736001), the High-Tech Research and Development Program of China (2006AA09A209–5), the Major State Basic Research Development Program of China (2009CB219507) and the Fundamental Research Funds for the Central Universities of China.

* Corresponding author.
E-mail address: powere@dlut.edu.cn (Y. Song).

0730-725X/$ – see front matter © 2011 Elsevier Inc. All rights reserved.
doi:10.1016/j.mri.2011.04.008

the liquid water protons with high space resolution in three dimensions. In order to obtain high-precision data and make visible measurement, MRI has been used for studying the hydrate. Having designed and constructed a high-pressure vessel to safely withstand 40 MPa, Hirai et al. [14] observed CO_2 hydrate growth in a water droplet injected into liquid CO_2 at 20 MPa with the vessel. Their experiments demonstrated not only the effective performance of the apparatus but also the perfect performance of MRI for hydrate investigations. Then they measured hydrate thickness growth with MRI and the phenomenon applied to advanced CO_2 ocean dissolution technology [15]. They concluded that CO_2 droplets dissolve during the process of sinking from their release point into deep ocean, by forming fine hydrate particles inside CO_2 droplets. The distribution of supercritical CO_2 injected into a packed bed of glass beads containing water was also directly visualized by them using MRI [16].

The presence of porous medium posed a challenge for the hydrate investigation using MRI, but the baffle quickly disappeared with the work of Baldwin et al. [17]. They measured the formation and dissociation of tetrahydrofuran/water hydrate at ambient pressure. The formation and dissociation were monitored both in a Berea sandstone plug and in bulk. In both cases, they found that nucleation was needed to begin the formation process. Dissociation appeared to be dominated by the rate of thermal energy transfer. The dissociation temperature of hydrate formed in the sandstone plug was not significantly different from the dissociation temperature in bulk.

Kvamme et al. [3] applied MRI to visualize the conversion of CH_4 hydrate within the Bentheim sandstone matrix into the CO_2 hydrate. And then Stevens et al. [18] carried a number of laboratory experiments to investigate the rates and mechanisms of hydrate formation in coarse-grain porous media. Many of these experiments were conducted in a sample holder fitted within a MRI instrument that allowed for a unique method of monitoring hydrate formation by the loss of signal intensity as water and free gas are converted into a solid phase. The rates and efficiency of the exchange process were reproducible over a series of initial conditions, with the notable observation that no free water was observed during the exchange process. Permeability measurements on hydrate saturated core indicate a finite level of permeability to gas, even in cores where all of the free water was converted to hydrate. Most of the following experiments done by them were also focused on the exchange of carbon dioxide for methane in the hydrate [19–22]. Nuclear magnetic resonance (NMR) spectroscopy is also an effective method to investigate the dissociation behavior of the CH_4 +CO_2 binary gas hydrate [23]. This technique can be used to distinguish the hydrate structure present, as well as to quantify phase concentrations.

Although a number of studies have been carried to investigate hydrate using MRI, there is only very limited information on CO_2 hydrate in porous medium. After obtaining experimental data of CO_2 hydrate formation and dissociation in a porous medium using MRI [24], the purpose of this study was to analyze the different dissociation rate of CO_2 hydrate using two heating rates. In this study, CO_2 hydrate was firstly formed in a porous medium using a high-pressure vessel and then it was dissociated using two heating rates. The water MRI mean intensity and the pressure of the vessel were both recorded during hydrate formation and dissociation. The CO_2 hydrate formation and dissociation rate were quantified using the MRI mean intensity of water.

2. Experimental investigation

2.1. Experimental apparatus

The experimental apparatus consisted of five subsystems (Fig. 1): (A) the high-pressure vessel; (B) the MRI system to visualize CO_2 hydrate formation and dissociation; (C) the data acquisition system to measure pressure and temperature; (D) water and carbon dioxide high-pressure pumps to provide pore pressure; (E) and a low-temperature cooling system to keep the vessel at low temperature.

An important criterion of the high-pressure vessel is that it must be made of nonmagnetic material and have a relatively large inside volume. The vessel is made of polyimide and its design pressure is 12 MPa. It is cylindrical in symmetry with a total size of Φ38×314 mm, and the effective size for packed glass beads is Φ15×200 mm. There is a jacket around the vessel, where the coolant circulated.

The MRI operated at a resonance of 400 MHz, 9.4 T, to measure hydrogen. ^1H MRI produces images of hydrogen contained in liquids, but does not image hydrogen contained in solids such as crystal ice or the CO_2 hydrates because of their much shorter transverse relaxation times. The glass beads are not imaged because they are solid and contain little, if any, hydrogen. This makes MRI a potent tool to distinguish between solid hydrate and the liquid mixture from which the hydrate forms [15].

The pressure (produced by Nagano Co., Ltd., Japan) and temperature transducers (produced by Yamari Industries, Japan) are separately connected to the vessel and the vessel jacket, respectively. The estimated errors of pressure and temperature measurements are ±0.1 MPa and ±0.1 K, respectively. Temperature and pressure signals from thermocouples and pressure sensors are collected by an A/D module (produced by Advantech CO., Ltd. China) and sent to a computer, then the data are processed by a monitor and control generated system.

The high-pressure pump (D-250L, produced by Haian Oil Scientific Research Apparatus Co., Ltd., China) was used to increase pore pressure by injecting water or CO_2. In order to acquire a stable temperature, a large-scale and high-precision thermostat bath (F25-ME, produced by JULABO Labortechnik GmbH, Germany) filled with fluorocarbon (FC-40, supplied by 3M Company, USA) was introduced to control

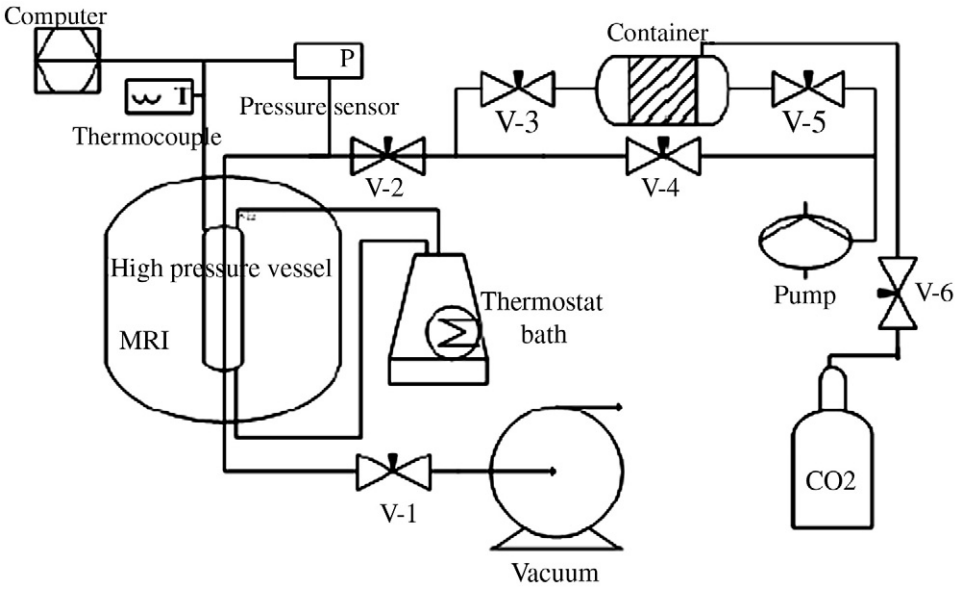

Fig. 1. Schematic diagram of the apparatus for monitoring and controlling pressure and temperature during carbon dioxide hydrate formation and dissociation.

temperature precisely, in which temperature is regulated and controlled by a heater and a refrigerator. The temperature stability of the thermostat bath was ±0.01 K.

2.2. Experimental procedures

The glass beads (diameter: 110 μm) used in this study were produced by As-One Co., Ltd., Japan. CO_2 (99.9%) was provided singly by Dalian Guangming Special Gas Co., Ltd., China. Deionized water was used in all the experiments. All chemicals were used without further purification.

After the glass beads were packed into the vessel tightly with deionized water (water saturation 100%), the vessel was reconnected to the experimental system and the deionized water was partly displaced with CO_2 gas (the water saturation changed to 50%). A vacuum pump was used to discharge the gas in the vessel, and CO_2 was then injected slowly into the vessel and pressure kept at the design value, 4.8 MPa. The vessel was then closed and kept at a steady temperature of 286 K which must be higher than the hydrate formation temperature to prevent hydrate formation at 4.8 MPa. The MRI began to obtain images when the bath temperature was decreased with a rate of 0.74 K/min. When hydrates formed in the vessel, the pressure change was observed due to sequestration of CO_2 in hydrate. The hydrate formation was considered to be finished when there was neither further pressure change nor image change. At 1 h, the bath temperature was increased gradually (1.6 K/min for Experiment 1 and 0.34 K/min for Experiment 2) to make the hydrate decompose. The vessel pressure and the MRI mean intensity were both recorded during the experiments.

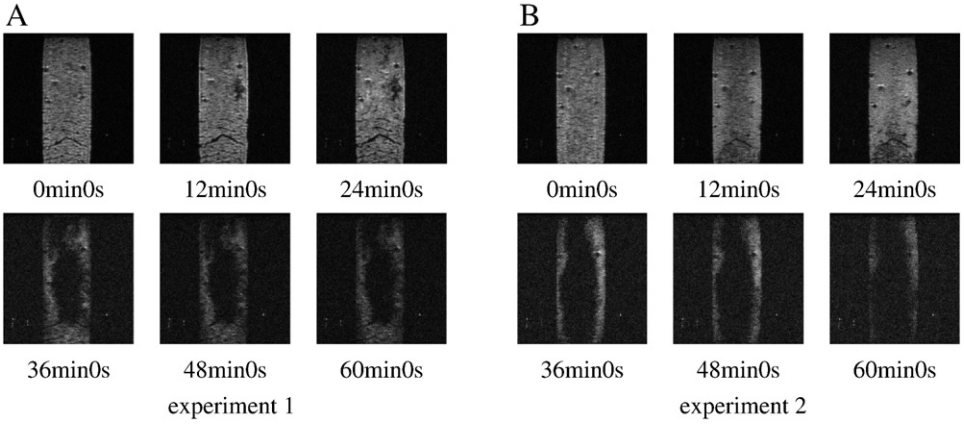

Fig. 2. Distribution of water saturation in the porous media during CO_2 hydrate formation with a cooling rate 0.74 K/min.

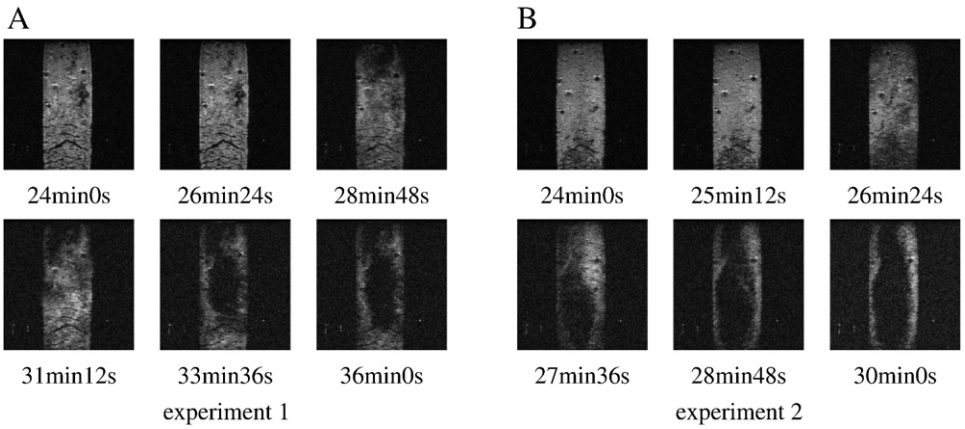

Fig. 3. Distribution of water saturation in the porous media when CO_2 hydrate formed abundantly with a cooling rate 0.74 K/min.

3. Results and discussion

3.1. Formation of CO_2 hydrate

The formation and dissociation of CO_2 hydrate in the porous medium were firstly visually investigated using MRI; the results were discussed in our previous work [24]. The sagittal plane was selected to display the experimental process in this study. The initial experimental pressure and temperature (p and T) were 286 K and 4.8 MPa, respectively; the temperature decrease rate of the vessel jacket was 0.74 K/min.

Fig. 2 shows the water distribution in the vessel during CO_2 hydrate formation. The bright signal in the images reflects the liquid water in the vessel. When liquid water was solidified (CO_2 hydrate was formed), the bright signal changed to dark in the images. The images showed that the initial formation site of CO_2 hydrate was along the axis of the vessel and then grew around. About 36 min later, the water distribution in the vessel was changeless, which implied the end of CO_2 hydrate formation in this experiment. The residual bright signal near the vessel wall indicated that the water was not totally consumed. The phenomenon was caused mainly by the formation of CO_2 hydrate which blocked some of the pores and prevented the contact of water and CO_2. As seen from Fig. 2, the formation rate was very high from 24 to 36 min for two experiments. This duration is particularly shown in Fig. 3, which indicated that the hydrate formation process was nearly finished in 2 min. The following conclusions can also be obtained in Fig. 3. The distribution of water signal in the vessel indicated that the hydrate formation rate for Experiment 2 was higher than that of Experiment 1. And the initial site of hydrate formation was also different from each other: vessel upside for Experiment 1 and vessel underside for Experiment 2.

The vessel pressure changes which imply the consumption and release of CO_2 during hydrate formation and dissociation for Experiment 1 are shown in Fig. 4. And the comparison of the MRI mean intensity of liquid water and the pressure in the vessel is also shown in it. The decrease of vessel pressure at the beginning of the cooling stage was caused by the decrease of temperature before the hydrate formation. After the temperature reached the designated value, about 30 min later, the decrease of MRI mean intensity and the increase of vessel pressure were mainly caused by the hydrate formation and phase change of CO_2 (from liquid phase to gaseous phase). During hydrate formation, the temperature was increased while the pressure was decreased, and at that time liquid CO_2 changed to gaseous CO_2 and caused pressure increase to counterbalance the pressure decrease. Since the CO_2 phase change rate from liquid to gaseous is higher than the CO_2 sequestration of hydrate formation, the experimental phenomena showed that p and T increase at the same time [25]. While the pore water was consumed during hydrate formation, the MRI mean intensity started to decrease. About 40 min later, hydrate formation was finished and the MRI mean intensity of water in the vessel was fairly constant throughout the experiment from 40 to 60 min. Since the comparison of the MRI mean intensity of liquid water and the vessel pressure for

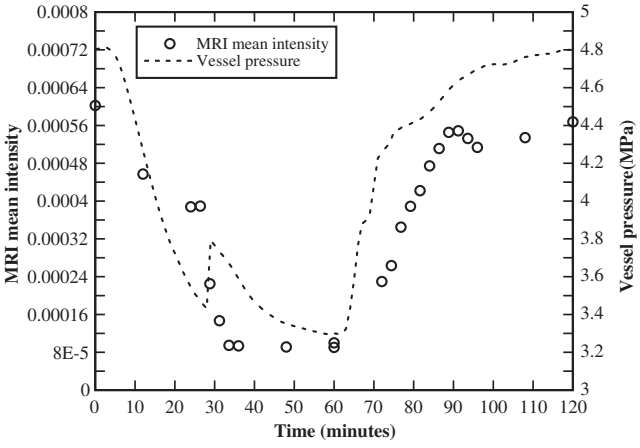

Fig. 4. MRI mean intensity of water and vessel pressure change during the formation and dissociation of CO_2 hydrate (Experiment 1: cooling rate, 0.74 K/min; heating rate, 1.6 K/min).

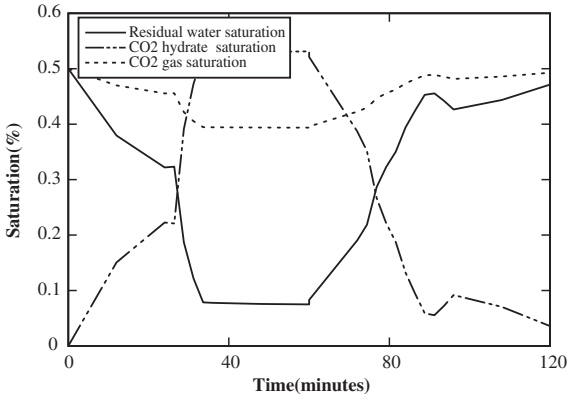

Fig. 5. Saturation of residual water, CO_2 hydrate and CO_2 gas during the formation and dissociation of CO_2 hydrate (Experiment 1: cooling rate, 0.74 K/min; heating rate, 1.6 K/min).

Experiment 2 was nearly the same as for Experiment 1, it was not discussed in this article.

The CO_2 hydrate formation and dissociation rate were also quantified using the MRI mean intensity of liquid water. The saturation of residual liquid water, CO_2 hydrate and CO_2 gas during the formation and dissociation of CO_2 hydrate of Experiment 1 is shown in Fig. 5. In this study, the initial water saturation was 50%. Saturation of residual liquid water can be calculated using MRI mean intensity. The expression of residual water saturation at i minutes (S_{Wi}) is shown as follows:

$$S_{Wi} = \frac{I_i \times S_{W0}}{I_0} \times 100\% \quad (1)$$

where S_{W0} is the initial water saturation and I_0 and I_i are the MRI mean intensity of liquid water at initial time and i minutes, respectively.

When brought to the earth's surface, 1 m^3 of gas hydrate releases 164 m^3 of natural gas and 0.8 m^3 of fresh water. So one volume of fresh water can form 1.25 volume of gas hydrates at standard temperature and pressure (STP) [26]. The saturation of CO_2 hydrate (S_{hi}) and CO_2 gas ($S_{CO_2,i}$) in the porous medium at i minutes can be calculated using the following equations:

$$S_{hi} = 1.25 \times \frac{(I_0 - I_i) \times S_{W0}}{I_0} \times 100\% \quad (2)$$

$$S_{CO_2,i} = 1 - S_{Wi} - S_{hi} \quad (3)$$

As seen from Fig. 5, the highest CO_2 hydrate saturation was 53% during Experiment 1 and the saturation of CO_2 gas is also shown in it. The change of CO_2 gas saturation was small from 40 to 60 min.

3.2. Dissociation rate of CO_2 hydrate with two heating rates

In this study, the heating rate was changed to investigate the effects of heating rate on CO_2 hydrate dissociation. The heating rate was 1.6 K/min for Experiment 1 and 0.34 K/min for Experiment 2. In the two experiments, the hydrates were heated starting at 60 min and, for convenience, the time was then set to 0 for discussion of the hydrate dissociation process. Fig. 6A shows the CO_2 hydrate dissociation process for Experiment 1 with a heating rate of 1.6 K/min, which was achieved by thermostat bath. The dissociation process was divided into six stages. As seen from Fig. 6A, the CO_2 hydrate began to dissociate in 12 min. Thirty-six minutes later, the CO_2 hydrate was nearly completed dissociated. Most of the hydrate dissociated from 12 to 24 min.

Fig. 6B shows the CO_2 hydrate dissociation process for Experiment 2, with a heating rate of 0.34 K/min, which was achieved by ambient conditions. The dissociation process was divided into 12 stages. As seen from Fig. 6B, the CO_2 hydrate began to dissociate in 36 min. About 120 min later, the hydrate was nearly dissociated completely. Much of the hydrate dissociated during 36 to 48 min. Comparison of Fig. 6A and B shows that the dissociation rate was affected by the heating rate.

The comparison of MRI mean intensity of liquid water and pressure of vessel with different heating rates is shown in Fig. 7. The heating rates have significant effects on the CO_2 hydrate dissociation. As seen from the MRI mean intensity

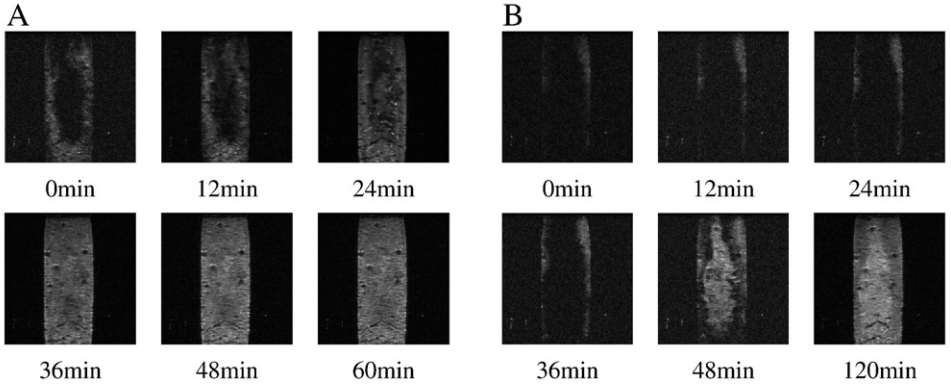

Fig. 6. Distribution of water saturation in the porous media during CO_2 hydrate dissociation process when the vessel was warmed with the following heating rates: (A) 1.6 K/min and (B) 0.34 K/min.

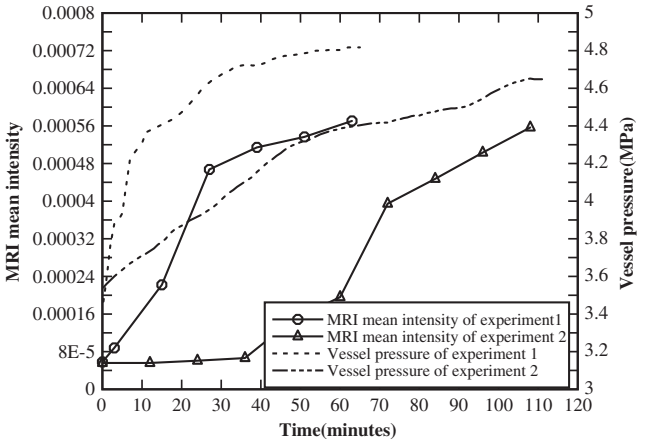

Fig. 7. Comparison of MRI mean intensity of liquid water and pressure of vessel during the CO_2 hydrate dissociation process with different heating rates (1.6 K/min for Experiment 1 and 0.34 K/min for Experiment 2).

of liquid water, the higher heating rate caused the rapid dissociation of the CO_2 hydrate, and the dissociation rate was kept nearly constant. The CO_2 hydrate dissociation was nearly finished 25 min later. When the heating rate was decreased to 0.34 K/min, the CO_2 hydrate began to dissociate after 38 min. Before this time the dissociation rate was very low, then the rate increased for a time to nearly the value for when the heating rate was 1.6 K/min, which took place about 65 min later for Experiment 2. The respective end of the CO_2 hydrate dissociation with two heating rates shows good agreement with each other.

There are lag times between pressure and MRI intensity during the CO_2 hydrate dissociation process, as shown in Fig. 7. The pressure reached the maximum value ahead of the MRI intensity for Experiment 1, and the result was absolutely different for Experiment 2. This phenomenon was mainly caused by the different size of the vessel (Φ15×200 mm) and the MRI field of view (FOV, 40×40×40 mm, the mean signal of which was used to calculate the MRI intensity of the sample). In other words, the FOV of MRI was only a part of the vessel and the pressure represents the value of the vessel.

The above experiments show that the initial formation sites of CO_2 hydrate are all near the axis of the vessel. This can be explained by the experimental preparation. Since the CO_2 gas was injected into the vessel last during the experimental procedures, the CO_2 gas will rest on the vicinity of the axis and the pore water will be driven to the position near the vessel wall. There was little CO_2 gas near these positions, so the pore water has less chance to interact with CO_2, and the formation of CO_2 hydrate is blocked.

3.3. Cracks in the porous medium during the heating process

When the vessel temperature was increased further during the heating process, cracks were found in the porous medium, as seen in Fig. 8. The cracks got bigger and bigger with the increasing temperature. Since there was no CO_2 hydrate in the vessel at this p–T condition, the cracks were not caused by the formation of CO_2 hydrate. The solubility of CO_2 in the solution decreased with the temperature increase [27], and the pore water was pushed aside by the CO_2 released from the water when the vessel was heated persistently after the CO_2 hydrate dissociated completely. Because of the absence of water (which contains proton), the swarm of CO_2 caused the dark cracks in the vessel, where gaseous CO_2 has displaced most of the liquid water in porous medium. The cracks became smaller and smaller as the temperature decreased, and the cracks disappeared completely.

4. Conclusions

Since MRI is an effective tool for hydrate investigations, a series of experiments were carried out to study CO_2 hydrate formation and dissociation in a porous medium using it. A new vessel was designed to satisfy the demands of high pressure and with no influence on the magnetic signal used in the experiments. Images were obtained by using a fast spin-echo sequence, and field of view was set to 40×40×40 mm. The vessel pressure was recorded during hydrate formation and dissociation, which was used to compare with MRI mean intensity of liquid water. The results indicated that the

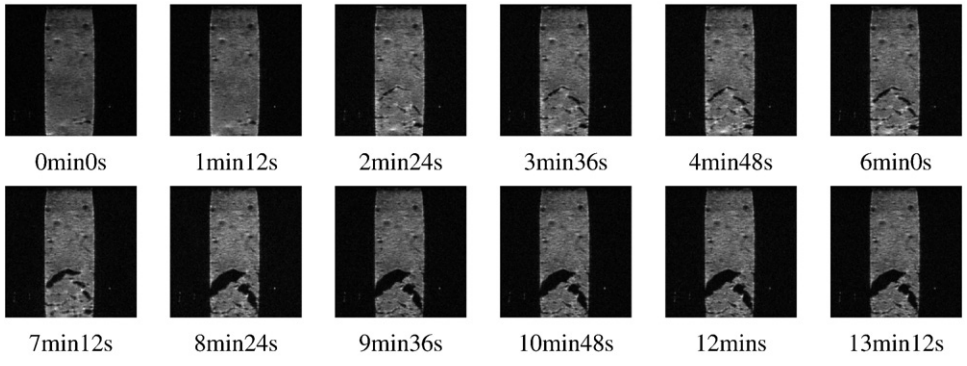

Fig. 8. Cracks in the porous medium when the vessel was heated persistently after the CO_2 hydrate dissociated completely.

MRI could visualize hydrate formation and dissociation. The comparison of MRI mean intensity of liquid water and pore pressure was in good agreement with each other to show the formation and dissociation process of CO_2 hydrate. The saturation of residual water, CO_2 hydrate and CO_2 gas during the formation and dissociation of CO_2 hydrate was calculated using MRI mean intensity of liquid water, which can indicate hydrate formation rate quantitatively. Two heating rates were used to dissociate the CO_2 hydrate, and the result showed that the higher heating rate caused rapid hydrate dissociation. Cracks were found in the porous medium during the formation and dissociation process, which was caused by the decrease of CO_2 solubility with the increasing temperature. The MRI technology is an effective tool for CO_2 hydrate investigation in porous medium.

References

[1] Yang HQ, Xu ZH, Fan MH, Gupta R, Slimane RB, Bland AE, et al. Progress in carbon dioxide separation and capture: a review. J Environ Sci 2008;20:14–27.

[2] Servio P, Englezos P. Effect of temperature and pressure on the solubility of carbon dioxide in water in the presence of gas hydrate. Fluid Phase Equilibria 2001;190:127–34.

[3] Kvamme B, Graue A, Buanes T, Kuznetsova T, Ersland G. Storage of CO_2 in natural gas hydrate reservoirs and the effect of hydrate as an extra sealing in cold aquifers. Int J Greenhouse Gas Control 2007;1: 236–46.

[4] Brewer PG, Orr FM, Friederich G, Kvenvolden KA, Orange DL. Gas hydrate formation in the deep sea: in situ experiments with controlled release of methane, natural gas and carbon dioxide. Energy Fuels 1998;12:183–8.

[5] Brewer PG, Friederich G, Peltzer ET, Orr FM. Direct experiments on the ocean disposal of fossil fuel CO_2. Science 1999;284:943–5.

[6] Brewer PG, Peltzer ET, Friederich G, Aya I, Yamane K. Experiments on the ocean sequestration of fossil fuel CO_2: pH measurements and hydrate formation. Mar Chem 2000;72:83–93.

[7] Brewer PG, Peltzer ET, Friederich G, Rehder G. Experimental determination of the fate of rising CO_2 droplets in sea water. Environ Sci Technol 2002;36:5441–6.

[8] Koide H, Shindo Y, Tazaki Y, Iijima M, Ito K, Kimura N, et al. Deep sub-seabed disposal of CO_2—The most protective storage. Energy Convers Mgml 1997;38:253–8.

[9] Aya I, Yamane K, Shiozaki K. Proposal of new COSMOS, CO_2 Sending Method for Ocean Storage, basing on an in situ experiment with MBARI. In: 24th Meeting of UJNR Marin Facilities Panel, Honolulu. 2001.

[10] Aya I, Yamane K, Shiozaki K, Brewer PG, Peltzer E. Proposal of slurry type CO_2 sending system to the ocean floor, new COSMOS. Fuel Chem Div Prepr 2002;47:27–33.

[11] Lee SY, Liang LY, Riestenberg D, West OR, Tsouris C, Adams E. CO_2 Hydrate composite for ocean carbon sequestration. Environ Sci Technol 2003;37:3701–8.

[12] Saji A, Noda H, Takamura Y, Tanii T, Takata T, Kitamura H, et al. Dissolution and sedimentation behavior of carbon dioxide clathrate. Energy Convers Manag 1995;36:493–6.

[13] Yamasaki A, Wakatsuki M, Teng H, Yanagisawa Y, Yamada K. A new ocean disposal scenario for anthropogenic CO_2: CO_2 hydrate formation in a submerged crystallizer and its disposal. Energy 2000;25: 85–96.

[14] Hirai S, Kuwano K, Ogawa K, Iriguchi N, Okazaki K. High-pressure magnetic resonance imaging up to 40 MPa. Magn Reson Imaging 2000;18:221–5.

[15] Hirai S, Tabe Y, Kuwano K, Ogawa K, Okazaki K. MRI measurement of hydrate growth and an application to advanced CO_2 sequestration technology. Ann N Y Acad Sci 2000;912:246–53.

[16] Suekane T, Soukawa S, Iwatani S, Tsushima S, Hirai S. Behavior of supercritical CO_2 injected into porous media containing water. Energy 2005;30:2370–82.

[17] Baldwin BA, Moradi-Araghi A, Stevens JC. Monitoring hydrate formation and dissociation in sandstone and bulk with magnetic resonance imaging. Magn Reson Imaging 2003;21:1061–9.

[18] Stevens JC, Howard JJ, Baldwin BA, Ersland G, Husebø J, Graue A. Experimental hydrate formation and gas production scenarios based on CO_2 sequestration. Proceedings of the 6th International Conference on Gas Hydrates (ICGH), Vancouver, British Columbia, Canada. 2008.

[19] Husebø J, Ersland G, Graue A, Kvamme B. Effects of salinity on hydrate stability and implications for storage of CO_2 in natural gas hydrate reservoirs. Energy Procedia 2009;1:3731–8.

[20] Ersland G, Husebo J, Graue A, Kvamme B. Transport and storage of CO_2 in natural gas hydrate reservoirs. Energy Procedia 2009;1: 3477–84.

[21] Ersland G, Husebo J, Graue A, Baldwin BA, Howard J, Stevens J. Measuring gas hydrate formation and exchange with CO_2 in Bentheim sandstone using MRI tomography. Chem Eng J 2009;158:25–31.

[22] Baldwin BA, Stevens J, Howard JJ, Graue A, Kvamme B, Aspenes E, et al. Using magnetic resonance imaging to monitor CH_4 hydrate formation and spontaneous conversion of CH_4 hydrate to CO_2 hydrate in porous media. Magn Reson Imaging 2009;27:720–6.

[23] Rovetto LJ, Dec SF, Koh CA, Sloan ED. NMR studies on CH_4+CO_2 binary gas hydrates dissociation behavior. Proceedings of the 6th International Conference on Gas Hydrates, Vancouver, British Columbia, Canada. 2008.

[24] Yang MJ, Song YC, Zhao YC. MRI measurements of CO_2 hydrate formation and dissociation in porous medium. The 20th International Offshore and Polar Engineering Conference & Exhibition. Beijing, PR China. 2010.

[25] Yang MJ, Song YC, Liu Y. Equilibrium conditions for CO_2 hydrate in marine sediment environment. J Chem Thermodyn 2011;43:334–8.

[26] Sloan ED. Clathrate hydrates of natural gases. New York: Marcel Decker; 1998.

[27] Song YC, Chen BX, Shen SQ. Density and state function of CO_2 salt water solution in underground condition. J Therm Sci Technol 2003;2: 358–64.